Korean J. Chem. Eng., 35(12), 2487-2495 (2018)
DOI: 10.1007/s11814-018-0153-2

pISSN: 0256-1115
eISSN: 1975-7220

Improved performance of polyamide nanofiltration membranes by incorporating reduced glutathione during interfacial polymerization

Zhiwei Jiao*,, Linjie Zhou*,**, Mengyuan Wu*,**, Kang Gao*,**, Yanlei Su*,**,†, and Zhongyi Jiang*,****

*Key Laboratory for Green Chemical Technology, School of Chemical Engineering and Technology, Tianjin University, Tianjin 300072, China
**Collaborative Innovation Center of Chemical Science and Engineering (Tianjin), Tianjin University, Tianjin 300072, China
(*Received 23 October 2017 • accepted 18 September 2018*)

Abstract-Inspired by the specific amino acid sequence Asn-Pro-Ala (NPA) of water channel aquaporins (AQPs), we fabricated polyamide (PA) nanofiltration (NF) membranes by introducing reduced glutathione (GSH) in interfacial polymerization (IP) method. Fourier transform infrared spectroscopy (ATR-FTIR), X-ray photoelectron spectrometry (XPS), scanning electron microscope (SEM), atomic force microscopy (AFM), zeta potential and static water contact angle measurement were employed to characterize the chemical composition, morphology, electronegativity and hydrophilicity of the NF membranes. The water flux of GSH/PIP-TMC NF membrane reached 32.00 L m^{-2} h^{-1} at 0.2 MPa, which was approximately twice than that of pristine PIP-TMC NF membrane when the ratio of GHS to piperazidine (PIP) was 40% during IP process. More water channels were built as GSH was embedded into PA layer. The fabricated NF membranes also took on potent rejection for dyes and Na_2SO_4. This study presents a simple and facile method to simulate water channels-based biological materials which may find potential application in water treatment.

Keywords: Reduced Glutathione, Water Channels, Interfacial Polymerization, Nanofiltration Membrane

INTRODUCTION

Water scarcity counts as one of the largest global issues due to population growth, misuse, industrialization and climate change [1,2]. To tackle this issue, efficient and sustainable technologies are urgently required for the supply of fresh water in considerable amount. In recent years, the membrane-based process has aroused much attention in water purification and desalination processes [3,4]. Aquaporins (AQPs), membrane proteins ubiquitous in the cells of organisms, take on notably high water permeability and rejection of protons, ions and neutral solutes. Due to its potent selectivity, different types of AQPs biomimetic membranes with high selectivity and permeability have been fabricated by introducing proteoliposomes or proteopolymersomes onto the supporting membranes.

Polymeric membranes were prepared by Kumar et al. [5] by introducing Aquaporin Z (AqpZ) into amphiphilic triblock-polymer vesicle. The as-prepared membranes took on a water permeation flux that was approximately one order of magnitude higher than the existing membranes and complete rejection of glucose, glycerol, salt and urea. By using immobilized AqpZ lipid bilayer (SLB) as filler material, Wang et al. [6] successfully applied layer-by-layer (LbL) method to fabricate a novel nanofiltration (NF) membrane. The resultant membranes displayed a huge flux and excellent rejection to univalent and multivalent salts. Zhao et al. [7] reported reverse osmosis (RO) membranes via interfacial polymerization (IP) between m-phenylene diamine (MPD) and trimesoyl chloride (TMC) with AQP-based proteoliposomes as aqueous solution additive, which exhibited superior water permeability and were approximately 40% higher than the commercial RO membrane. The operational complexity and high cost make it impossible for large-scale applications, though AQPs-based biomimetic membranes have shown unexceptionable permeability and selectivity [8-10]. To solve this problem, simple compounds such as biologic materials can be selected to systematically design biomimetic membranes.

Reduced glutathione consists of glutamic acid, cysteine and glycine, which plays multiple critical functions *in vivo*, such as detoxification to some heavy metals, transport of cysteine and gene expression [11-13]. GHS has a similar amino acid sequence with selectivity filters of AQP1. The interactions between amino acid and water molecules notably affect the process of water transport in the filters of AQP1. Besides, Asn-Pro-Ala (NPA) and aromatic-arginine (ar/R) constrictions are formed in the selectivity filters of AQP1, which are critical for selective permeation of water molecules, ions and protons [14]. Besides, the transport of water in the AQP1 also depends on the hydrogen-bond-forming groups, which primarily originate from residues histidine (H) 182, arginine (R) 192 and carbonyl oxygens of residues G190, C191 and G192 [15].

Recently, several approaches, such as solution casting [16,17], solution coating [18], IP [19,20], have been employed to fabricate NF membranes. Solution casting is a conventional process where multifunctional nanomaterial or macromolecule is blended into polymer matrix, followed by phase inversion method to form NF membrane. Nevertheless, the polymer matrix and inorganic material are often poorly compatible, leading to poor dispersion and aggrega-

†To whom correspondence should be addressed.
E-mail: suyanlei@tju.edu.cn

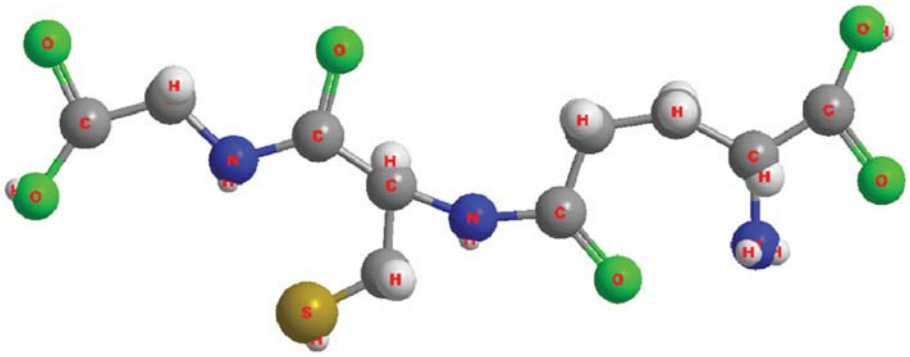

Fig. 1. The ball-stick model of GHS molecule.

tion of nanoparticles, which is detrimental to phase inversion process as decreasing the separation performance of membrane [21]. Normally, solution coating is a strategy by which viscous solution is coated onto the surface of the supporting membrane to construct a selective layer. However, coating solution may permeate into the macropores of the supporting membrane rather than forming a selective layer [22]. Besides, the thickness of the separation layer could be tens of micrometers, which could hinder the penetration of water molecules through the membrane. Accordingly, a low flux is caused. IP is an economical method to fabricate NF membrane as compared with solution casting and solution coating, by which polymerization takes place at the interface between water and organic phases under mild conditions [23]. To obtain superb separation performance, the thin layer and supporting membrane can be designed independently [24]. To our best knowledge, no work has been reported about embedding biomaterial-peptide into NF membrane.

Given this, we introduced GHS into polyamide (PA) membranes via IP method as inspired by the special amino acid sequence NPA of AQPs, and filtration efficiency of the GHS/PIP-TMC NF membranes was increased. The difference between this work and the previous one primarily lies in two aspects. On the one hand, we embedded parallel structure-GHS into PA layer in the IP process as inspired by the superstructures of AQPs, which was expected to increase the performance of the membrane. On the other hand, GHS could disturb the formation of dense PA network formed by crosslinking between PIP and TMC. This could cause the NF membranes to possess a comparatively loose PA layer, and subsequently increase the permeation performance of the membrane. Yet the addition of GHS did not cause evident structural defect of the active layer.

EXPERIMENTS

1. Materials

Polyethersulfone (PES, *Mw*=29,000) was offered by BASF Co. (Germany) and pretreated in the vacuum oven at 110 °C for 24 hours before us; Poly (ethylene glycol) (PEG, *Mw*=2,000), Trimesoyl chloride (TMC, *Mw*=265.43) and Orange GII (orange G, *Mw*=452.37) were purchased from Aladdin Reagent Database Inc. (Shanghai, China). Piperazidine (PIP, *Mw*=86.14), Congo red (*Mw*=696.68), Methyl blue (*Mw*=799.81), NaCl, Na_2SO_4, $MgCl_2$ and $MgSO_4$ were supplied by Guangfu Fine Chemical Technology Institute (Tianjin, China). N, N-dimethylformamide (DMF) and n-heptane were obtained from the Institute of Jiangtian Chemical Technology (Tianjin, China). Reduced glutathione (GSH, *Mw*=307.33) was procured from Heowns Biochem Technologies LLC (Tianjin, China). The ball-stick model of GHS molecule is presented in Fig. 1. All the data (inclusive of generic names, chemical names, structures, CAS numbers, purities and molecular weights) of the used dyes are listed in Table S1 and S2 (as provided in the supplementary materials). Deionized water was prepared by water purification systems in the lab.

2. Preparation of Nanofiltration Membranes

PES ultrafiltration membranes were first prepared by non-solvent induced phase separation (NIPS) method [25], as reported in our previous study. Polyamide (PA) NF membranes were produced following IP method. First, the PES supporting membranes were soaked into PIP aqueous solution for 10 min. GHS was also dissolved into amine monomer aqueous solution as additive. Next, impregnated membranes were extracted from amine monomers solutions, following eliminating excess solutions with filter papers. Then, the PIP- and GHS-saturated PES membranes were added to TMC solution to perform IP and the reaction time ranged from 0.5 to 3 min. The concentration of TMC in n-hexane ranged from 0.1 to 0.3 wt%. The NF membranes were dried in the vacuum oven at 60 °C for 15 min after the IP process to further react and fully evaporate n-hexane to form a dense PA layer. Eventually, the resultant membranes were stored in deionized water before use. Membranes were synthesized with 0.1 wt% concentration of TMC for ATR-FTIR, XPS, SEM, AFM, zeta potential and static water con-

Table 1. Static water contact angle of GHS/PIP-TMC NF membranes with different concentrations of water phase additive GHS

Membranes	TMC (wt%)	PIP (wt%)	Ratio of GHS to PIP (wt%)	Static water contact angle (°)
M_0	0.1	0.1	0	58.2±0.4
M_1	0.1	0.1	10	52.1±1.7
M_2	0.1	0.1	15	48.8±0.6
M_3	0.1	0.1	20	26.3±0.8
M_4	0.1	0.1	25	22.2±0.5
M_5	0.1	0.1	30	16.7±0.3
M_6	0.1	0.1	40	13.7±0.1

tact angle analysis, and reaction time was 2 min. These NF membranes are denoted in Table 1 to conveniently describe and study.

3. Characterization of Membranes

Surface chemical structures and functional groups of the membranes were anatomized using Fourier transform infrared spectroscopy (ATR-FTIR, Vector 22 FTIR spectrometer, Bruker Optics) running with air as background. Transmittance spectra were attained in the region of 4,000-500 cm^{-1} with resolution of 4 cm^{-1} for 64 scans.

X-ray photoelectron spectroscopy (XPS, Kratos Axis Ultra DLD) served to measure the surface compositions of membranes by employing Al Kα (1,486.6 eV) as the radiation source. By using an aperture slot of 300 μm×700 μm, all XPS spectra were recorded, and the collected survey spectra ranged from 0 eV to 1,100 eV. The takeoff angle of the photoelectron was set at 90°.

Field emission scanning electron microscope (FESEM, Nanosem 430) was used to characterize the surface and cross-section morphologies of the NF membranes. The membranes were frozen through vacuum freeze-drying and sputtered with gold before SEM observation. Surface roughness in 10 μm×10 μm area of the membrane surface was measured following atomic force microscopy (AFM, Multimode 3, Bruker Co.) as operated in a contact mode.

The hydrophilicity of the membrane surface was measured by static contact angle measurement (JC2000C Contact Angle Meter, Powereach Co., Shanghai, China). First, filter papers were used to dry the surface of the membrane, then a droplet of deionized water was dropped with volume of 4 mL on the membrane surface. At least five sites contact angles at one sample were measured, and the average was referenced to acquire a reliable value.

To measure the surface charge of the membranes, Electro Kinetic Analyzer (Austria/Anton Paar KG, Austria) was used at pH=6.0± 0.2 with KCl solution (0.001 M) circulating through the measuring cell, and the value of the zeta potential was calculated by using the Helmholtz-Smoluchowski equation.

4. Separation Properties of NF Membranes

The separation properties of the fabricated NF membranes were studied by using laboratory scale dead-end filtration system consisting of a filtration cell (model 8200, Millipore Co.). This filtration cell is equipped with a volume capacity of 200 mL solution reservoir and connected with a nitrogen gas cylinder. The filtration area of this system reaches 28.7 cm^2. The filtration cell setup is illustrated in Fig. S1 (as presented in the supplementary materials). To acquire stable value of the water flux before test, each membrane was prepressed with deionized water under 0.25 MPa for 30 min. Next, the pressure was adjusted at 0.2 MPa to evaluate the properties of the NF membranes. The concentrations of inorganic salts (NaCl, Na_2SO_4, $MgCl_2$, $MgSO_4$) and dyes (Orange GII, Congo red, Methyl blue) in aqueous solutions were 1.0 g L^{-1} and 0.1 g L^{-1}, respectively. The equation below was used to calculate the flux of the membrane:

$$J = \frac{V}{A\Delta t} \tag{1}$$

where J (L m^{-2} h^{-1}) denotes the water flux and V (L) represents the volume of permeated water. A (m^2) refers to the membrane area, and Δt denotes the permeation time.

The value of rejection (R) was calculated by the equation as follows:

$$R = \left(1 - \frac{C_p}{C_f}\right) \times 100\% \tag{2}$$

C_p and C_f refer to the concentrations of permeate and feed solutions. The concentrations of inorganic salts and dyes were measured by electrical conductivity (DDS-11A, Shanghai Leichi Instrument Co., Shanghai, China) and UV-vis spectrophotometer (Hitachi UV-2800, Hitachi Co., Japan), respectively.

RESULTS AND DISCUSSION

1. Characterization of NF Membranes

To a certain extent, the specific amino acid sequence of GSH resembled NPA of AQPs. A simple and facile method was proposed to simulate water channels. GHS/PIP-TMC NF membranes were

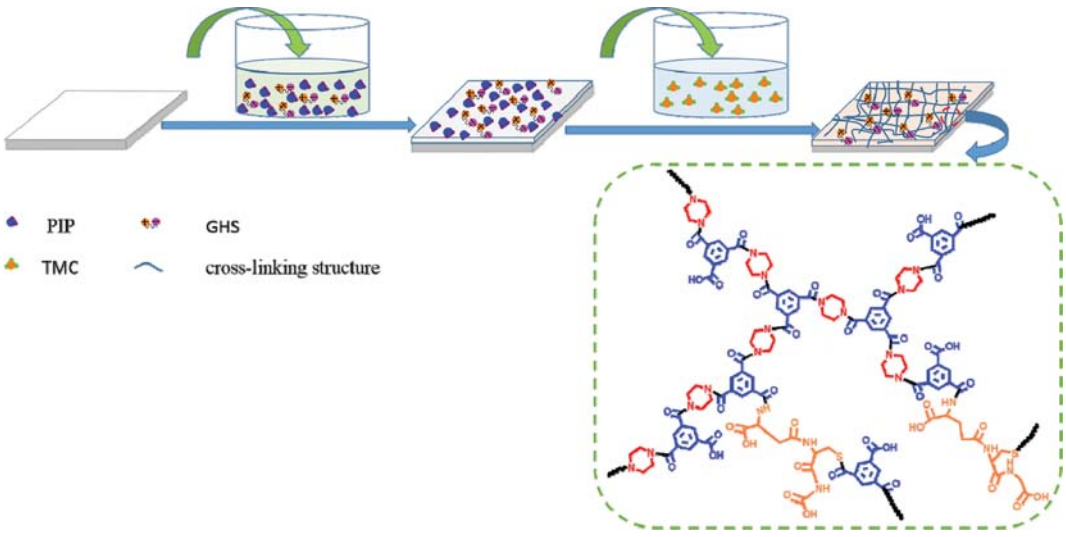

Fig. 2. Schematic diagram to explicate the preparation process of GHS/PIP-TMC NF membranes.

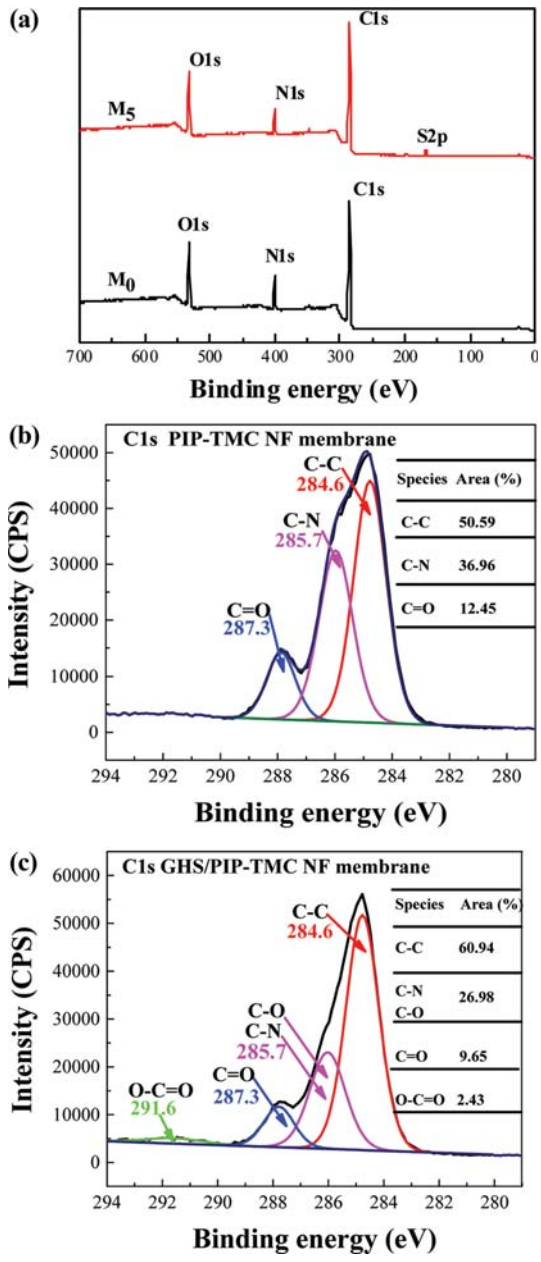

Fig. 3. (a) XPS wide-scan spectra of PIP-TMC NF membrane (M_0) and GHS/PIP-TMC NF membrane (M_5); High-resolution C 1s core level spectra of (b) PIP-TMC NF membrane (M_0), (c) GHS/PIP-TMC NF membrane (M_5).

fabricated by introducing GSH via IP method. A schematic diagram to explicate the preparation process of GHS/PIP-TMC NF membranes is presented in Fig. 2. The PES supporting membrane was first immersed into PIP aqueous solution with GHS as the co-reactant. Polyamide (PA) layers were then fabricated on the surface of the immersed membrane through cross-linking reaction. The introduction of GSH formed more water channels in the PA thin layer.

The variations in chemical structures of the active layer of the NF membranes were followed by ATR-FTIR, as presented in Fig. S2 (as provided in the supplementary materials). A characteristic peak appeared at 1,625 cm^{-1} of PIP-TMC (M_0) and GHS/PIP-TMC NF membranes (M_3, M_5), which was consistent with the stretching vibration peak of C=O bond of the amide group. To further characterize the surface compositions and element contents of the membranes, XPS was adopted. XPS wide-scan spectra of the PIP-TMC NF membrane (M_0) and GHS/PIP-TMC NF membrane (M_5) are presented in Fig. 3(a), and the element contents are listed in Table 2. A new element S appeared in the GHS/PIP-TMC NF membrane (M_5) compared with PIP-TMC NF membrane (M_0), which demonstrated that GHS was successfully embedded into the PA layer. Given that detection deepness of XPS technology was about 10 nm [26] which was thinner than the PA layer, no S element in the supporting membrane was found in the spectra of PIP-TMC NF membrane (M_0).

Table 2. Surface atomic compositions of PIP-TMC NF membrane (M_0) and GHS/PIP-TMC NF membrane (M_5)

Membranes	Atomic composition (at%)			
	C	O	N	S
M_0	75.38	15.03	9.59	0
M_5	73.16	15.74	8.96	2.14

Results of high-resolution C 1s core level spectra are illustrated in Fig. 3(b) and (c). These suggested the possible interaction between GHS and PA layer, and evaluated the variation of cross-linking degree of PA layer. The deconvolution of N1s and O1s is also presented in Fig. S3 (as provided in the supplementary materials). The deconvolution of C 1s peak generated three characteristic peaks at 284.6, 285.7 and 287.3 eV in terms of PIP-TMC NF membrane (M_0), denoting C-C, C-N and C=O bonds, respectively. Similar peaks were found in the C 1s core level spectra of GHS/PIP-TMC NF membrane (M_5) except at 291.6 eV and corresponded to O-C=O bond, which might stem from the carboxyl group on GHS. The notable decrease of C-N bond content (from 36.96% of M_0 to less than 26.98% of M_5) implied the decline of cross-linking degree of PA layer as GHS interfered the reaction between PIP and TMC (through forming covalent bond), which formed the comparatively loose NF membrane.

The surface and cross-section morphologies of the membranes were observed by SEM. The surface of PIP-TMC NF membrane took on typical nodular structure, which was attributed to the macromolecules formed by crosslinking between PIP and TMC [27], as presented in Fig. 4(a)-(b). Visible nodular and spherical globule structures would become more obvious on the surface of membranes from M_1 to M_5, as the doping concentration of GHS increased. Zhu et al. [20] also reported a similar structure on the surface of PIP-TMC NF membrane. This might stem from the embedment of hydrophilic GHS, which generated the intermolecular hydrogen bonding in the cross-linking PA chains, and the intermolecular hydrogen bonding played a dominant role in the formation of the spherical globule structure [28]. Particularly, highly stacked cobble structures were uniformly distributed on the surface of the resultant membrane (M_6) under the ratio of GHS to PIP as 40%, as also observed by previous research as well [29]. However, in Fig. 4(b), no notable variation of the cross-section morphology was ob-

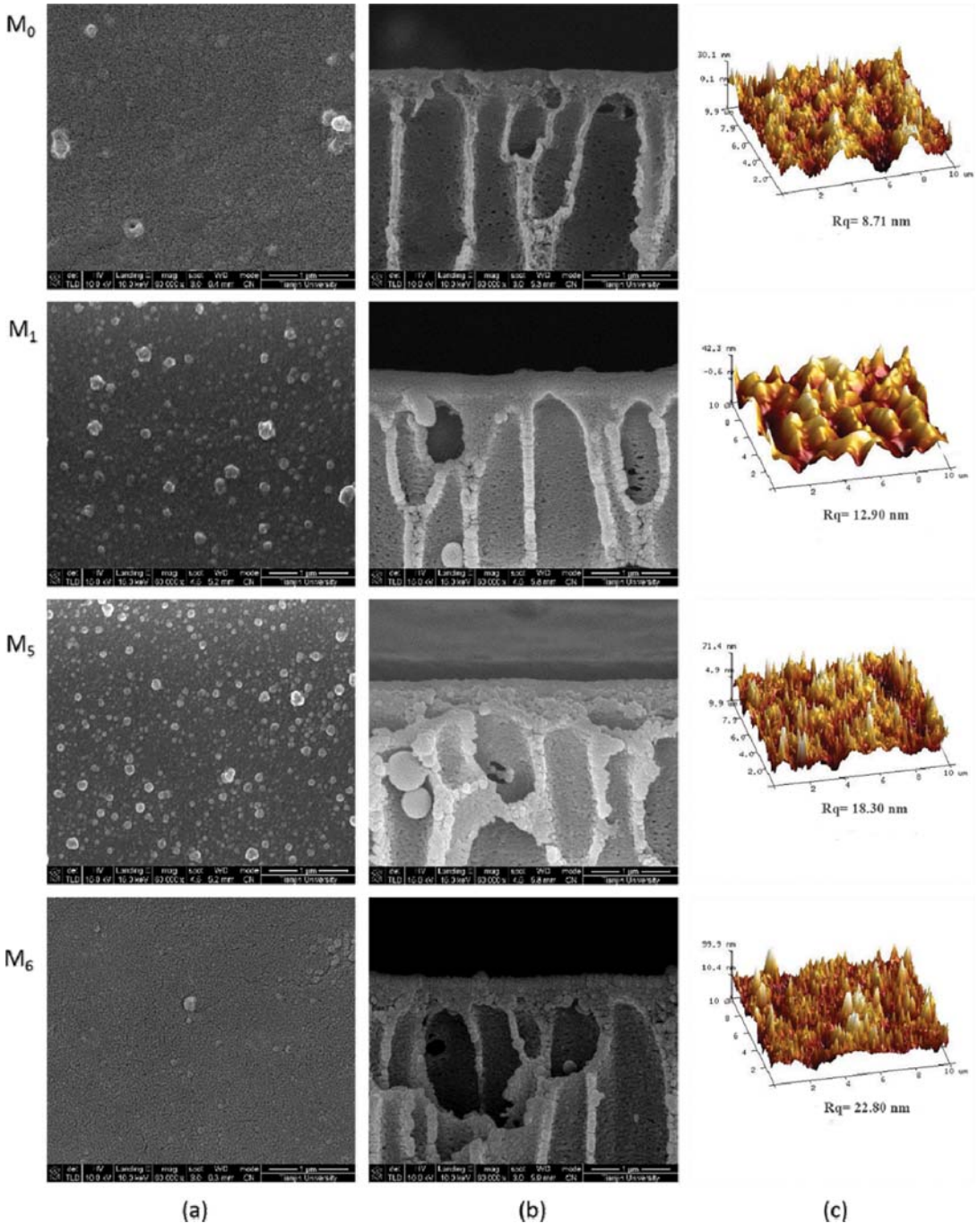

Fig. 4. Surface and cross-section morphologies of the PIP-TMC NF membrane (M_0) and GHS/PIP-TMC NF membranes (M_1, M_5, M_6).

served after the GHS was introduced into the PA layer, which was encompassed by the PA layer and porous PES supporting membrane.

AFM analysis was performed to further measure the surface roughness of the NF membranes, and the 3D images are presented in Fig. 4(c). The PIP-TMC NF membrane (M_0) took on the lowest surface roughness and the value of the root mean square roughness (RMS) was 8.71 nm. The RMS value rose from 12.9 to 22.8 nm as the ratio of GHS to PIP increased from 10 to 40%. In previous study, the surface roughness of NF membrane was associated with the structure of the PA layer, and the surface structure and interfacial properties of the membrane were bound by the chemical structure, concentration, diffusivity and solubility of amine monomer [24]. GHS has not only asymmetric reactive amino and sulfhydryl groups, but also a long chain as compared with alicyclic amine monomer PIP, which can react with TMC and yield PA layer with a comparatively low cross-linking degree. Besides, the multi-orientation and free amide groups in the cross-linked PA chains also increased surface roughness [28], which led to the increase of the surface area, thus enhancing the water flux of membranes [30].

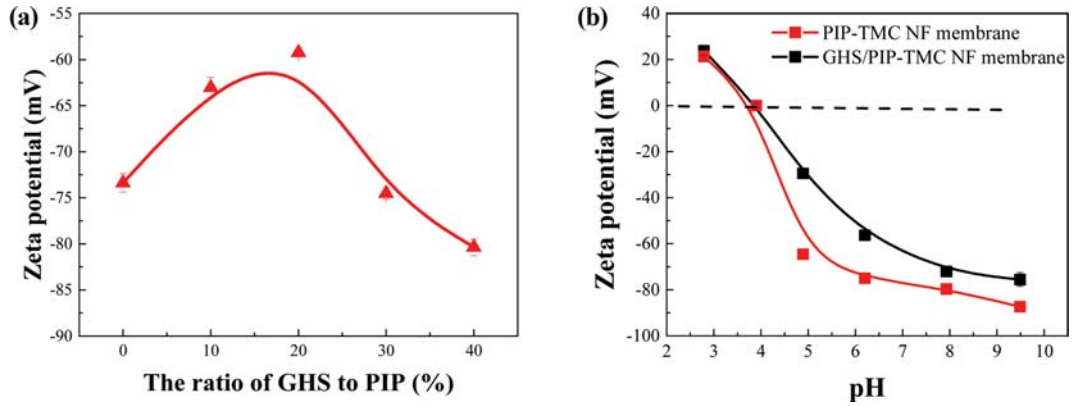

Fig. 5. (a) Zeta potential of GHS/PIP-TMC NF membranes with different concentrations additive GHS, (b) effect of pH on the zeta potential of PIP-TMC NF membrane (M_0) and GHS/PIP-TMC NF membrane (M_5).

The hydrophilicity of the membrane surface was measured by static contact angle measurement [20,29], and the result is presented in Table 1. With the increasing addition of GHS, the values of the static water contact angle of the NF membranes decreased. The initial hydrophilic PIP-TMC NF membrane possessed low static water contact angle with the value of 58.2±0.4°. The lowest static water contact angle was attained by GHS/PIP-TMC NF membrane (M_6) and the value reached 13.7±0.1° under the ratio of GHS to PIP as 40%, which demonstrates that GHS was successfully doped into the PA layer. Moreover, zwitterionic pairs were rich in the cross-linked PA chains, which bound free water molecules via strong electrostatic interaction and formed hydration layer [31-33]. Furthermore, the intermolecular hydrogen bonding in the cross-linked PA chains might also increase hydrophilicity of the membrane, which complied with the surface morphology of the GHS/PIP-TMC NF membranes.

The surface charge was confirmed by zeta potential measurement, and the values are presented in Fig. 5. All the GHS/PIP-TMC NF membranes took on negative charges at the pH=6.0±0.2, due to the deprotonation of the carboxyl groups that were generated from hydrolysis of acyl chloride groups of TMC [34], as Fig. 5(a) presents. The value of the zeta potential increased dramatically from initial −73.38 mV of the PIP-TMC NF membrane (M_0) to −59.24 mV of the GHS/PIP-TMC NF membrane (M_3). Zeta potential curves of this shape were explicated as follows. PIP and GHS could react with TMC and generate hydrogen chloride that probably protonated amine groups, thus increasing zeta potential value of the membrane. Nevertheless, with the ratio of GHS to PIP increasing from 20% to 40%, the value of zeta potential decreased from −59.24 mV to −80.37 mV. This was primarily attributed to the comparatively high addition of GHS carrying a large number of carboxylic groups, and deprotonation of carboxylic groups would be attributed to the falling of zeta potential. Besides, GHS endowed the cross-linked PA chains with more pendent carboxylic groups, also causing more negative charges of the membrane. pH_{PZC} of the fabricated membrane was taken by varying the pH of the solution which flowed through the surface of membranes. Zeta potential of NF membranes decreased with the increase of pH from 2.79 to 9.49, the isoelectric point of PIP-TMC and GHS/PIP-TMC NF membranes was at pH 3.69 and 3.90, respectively, as presented in Fig. 5(b).

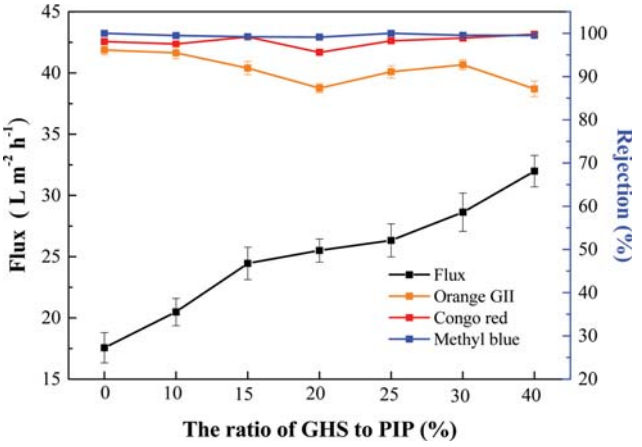

Fig. 6. Pure water flux and three different dyes rejections of GHS/PIP-TMC NF membranes with different concentrations of water phase additive GHS.

2. Effect of Preparation Conditions on the Separation Performance of NF Membranes

Permeability and selectivity count as two crucial parameters of NF membranes. Preparation conditions notably impact the separation performance of NF membranes, such as monomer concentration and reaction time. Thus, a series of experiments were performed to investigate these factors (TMC concentration and reaction time were fixed at 0.1 wt% and 2 min). The results are presented in Fig. 6. The PIP-TMC NF membrane exhibited low water flux with the value of 17.56 L m^{-2} h^{-1}. The water flux of GHS/PIP-TMC NF membrane increased almost twice, when the ratio of GHS to PIP was 40%. This could be attributed to the introduction of hydrophilic groups of carboxyl, amino, sulfhydryl and zwitterionic pair into the PA layer, which could better form a hydrated layer and build water channels in the PA layer.

In the NPA of AQPs, asparagine counts as a hydrogen bond donor and offers chemical groups transferring hydration of a certain water molecules and promoting water transportation. Herein, the function of GHS is just like asparagine in the NPA of AQPs.

Furthermore, GHS with carboxyl and amino groups is considered as zwitterion in the aqueous solution (pH=7.0). In this study, GHS could readily form typical structure of zwitterion after introducing GHS into the NF membranes, causing zwitterionic pair to arise in the cross-linking chains of the PA layer. Then, more water molecules covered the surface of the membrane via electrostatic interactions, which contributed to the formation of water channels and the transport of water molecules [35,36].

The rejection of dyes has undergone a decrease-increase-decrease process, which differs from the constant increase of water flux with the increasing addition of GHS. The pristine PIP-TMC NF membrane with high cross-linking degree had high rejection of dyes, which could be interpreted by steric hindrance effect [37]. The rejection of dyes decreased slowly as the ratio of GHS to PIP increased from 10 to 20%, which was attributed to continual decline of the extent of cross-linking of the PA layer. The rejection of dyes progressively increased until the ratio of GHS to PIP was 20%. This could be probably explicated that the cross-linking degree of GHS/PIP-TMC NF membranes increased under a comparatively high concentration of GHS. However, the rejection of Orange GII was high with the value of 92.74% under the ratio of GHS to PIP as 30%, and then the rejection of dyes started to decrease once again. The underlying cause is that GHS competed with PIP and reacted with TMC to form cross-linking structure, and the competition became strong under high concentration of GHS. Whereas, that GHS reacted with TMC could not form a dense PA layer compared with PIP. The ratio of GHS was fixed to PIP at 30% in the following experiments given the proper permeability and separation properties of GHS/PIP-TMC NF membranes.

Furthermore, the performance of NF membranes was impacted by TMC concentration in the organic phase. As shown in Fig. 7, the water flux decreased dramatically as the concentration of TMC increased from 0.05 to 0.1 wt%, then no obvious fluctuation appeared with the concentration of TMC further increasing to 0.3 wt%. While the rejection of Orange GII rose steadily from 76.41 to 98.27%, until the concentration of TMC reached 0.1 wt%, the rejection of Orange GII remained approximately constant with the further increasing concentration of TMC, which might be due to the fact

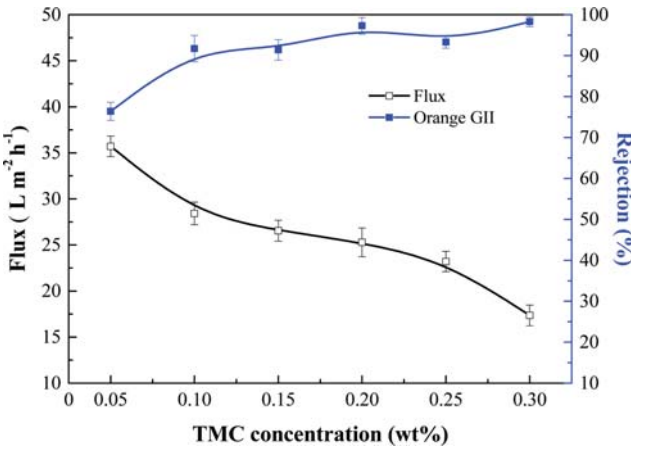

Fig. 7. Effect of TMC concentration on the performance of GHS/PIP-TMC NF membranes at 0.2 MPa.

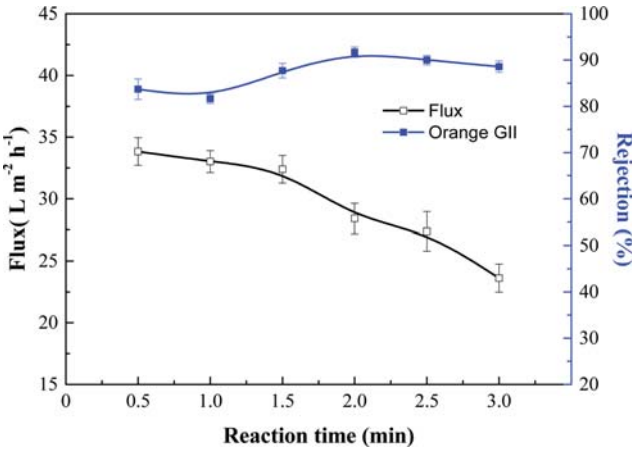

Fig. 8. Effect of reaction time on the performance of GHS/PIP-TMC NF membranes at 0.2 MPa.

that the extent of cross-linking of GHS/PIP-TMC NF membrane kept invariable under a comparatively high concentration of TMC. According to the result, the optimal concentration of TMC was 0.1 wt%.

Permeability and selectivity of the NF membranes were also affected by reaction time in the IP process. With the reaction time increasing from 0.5 to 2 min, the rejection of Orange GII increased slightly from 83.69 to 91.71%, as presented in Fig. 8. The rejection remained nearly unchanged when the reaction time was over 2 min. While water flux declined from 33.86 to 23.62 L m^{-2} h^{-1} with the reaction time prolonging from 0.5 to 3 min. The reason for this phenomenon could be described as follows. To our knowledge, IP process depends on the diffusion rate of amine monomer from the aqueous phase to the organic phase, which is self-inhibited [38,39]. Cross-linking degree of PA layer of the pristine NF membrane was low for a short time, which made this NF membrane high in permeability and poor in selectivity. The cross-linking degree increased, and the thickness of the PA layer became thick with the prolonged

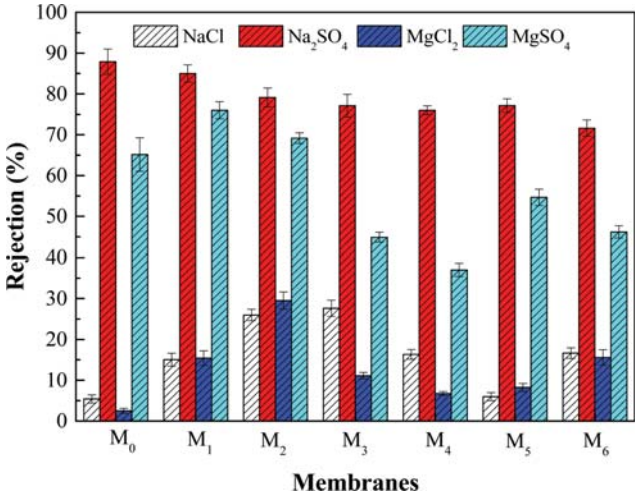

Fig. 9. Salt rejection performance of GHS/PIP-TMC NF membranes with different concentrations of additive GHS in the water phase.

Table 3. Performance comparisons among various modifiers for the fabrication of NF membranes in the previous reports and in this work

Membranes	Operation pressure (MPa)	Water flux (L m^{-2} h^{-1})	Salt rejection (%)	Dye rejection (%)	Ref.
GHS/PIP-TMC	0.2	32.0	Na_2SO_4 (80.0)	Congo Red (99.7)	This work
PIP/NH_2-PEG-NH_2	0.6	34.9	Na_2SO_4 (99.5)	-	[41]
NFM-AEPPS	0.6	43.1	K_2SO_4 (97.0)	-	[42]
CFGO/PA	1.0	110.4	Na_2SO_4 (84.0)	New Coccine (95.1)	[43]
NF-Jeffamine	0.4	35.5	$MgSO_4$ (73.0)	DOC (98.0)	[44]
NF-PSSNa/PVA	0.5	41.7	$MgSO_4$ (98.3)	Congo Red (99.7)	[45]
NF-$Al(OH)_3$	0.7	47.0	$MgSO_4$ (97.0)	-	[46]
TFN-MG-60	0.6	49.3	Na_2SO_4 (97.6)	-	[47]
TFN-NH_2-TNTs	0.7	52.5	Na_2SO_4 (96.4)	-	[48]
TFC-mm-BTEC	0.5	51.5	Na_2SO_4 (95.0)	-	[49]
mMSN/PA TFN	0.6	32.4	Na_2SO_4 (80.0)	-	[50]

reaction time, which caused consecutive decrease of the water flux and increase of the rejection ratio. Yet cross-linking degree and thickness of the PA layer did not increase with reaction time beyond 2 min owing to a self-limiting phenomenon. Thus, the optimal reaction time of this experiment was 2 min. The optimum preparation conditions in this experiment were as follows: TMC concentration, reaction time and the ratio of GHS to PIP were 0.1 wt%, 2 min and 30%, respectively.

The rejection of different salts of the GHS/PIP-TMC NF membranes is presented in Fig. 9. Rejection ratios of salt increased following the sequence of $MgCl_2$<NaCl<$MgSO_4$<Na_2SO_4 and could be explicated by Donnan exclusion theory [40], which complied with the values of zeta potential of the GHS/PIP-TMC NF membranes presenting negative charge under the experience condition. In this regard, electrostatic repulsive interaction between SO_4^{2-} and electronegative GHS/PIP-TMC NF membranes was stronger than that between Cl^- and these electronegative NF membranes. The potent rejection of Na_2SO_4 was realized, and the rejection reached approximately 80% under the ratio of GHS to PIP as 30%.

NF membranes modified by GHS in this work were compared with several reported membranes. Our membranes could be operated at an appropriate pressure, and improvement of water flux and comparable rejection of dyes and salts was observed, which would greatly cut costs in the industrial application, as suggested from Table 3. In conclusion, filtration efficiency of this NF membrane in terms of simultaneously obtaining proper permeability and selectivity was elevated by introducing GHS into the PA layers. Furthermore, these successfully fabricated bio-inspired membranes with biomimetic material would better develop artificial water channels and be introduced in the wastewater treatment.

CONCLUSIONS

A facile method to synthesize bio-inspired membranes was developed by introducing GHS into the PA layers following IP method. The function of GHS is just like asparagine in the NPA of AQPs, which promotes water transport in the PA layer. The permeate flux of the resultant NF membranes was twofold that of incipient membranes, and high rejection of dyes and salts was also realized. In brief, the incorporation of GHS into PA layer was beneficial to the enhancement of filtration efficiency of NF membranes. We hope this research will promote more materials for simulating the structure of AQPs to improve the performance of membranes.

ACKNOWLEDGEMENT

This research is supported by National Key Research and Development Program of China (No. 2016YFB0600503).

SUPPORTING INFORMATION

Additional information as noted in the text. This information is available via the Internet at http://www.springer.com/chemistry/journal/11814.

REFERENCES

1. A. Lee, J. W. Elam and S. B. Darling, *Environ. Sci. Water Res. Technol.*, **2**, 17 (2016).
2. M. A. Shannon, P. W. Bohn, M. Elimelech, J. G. Georgiadis, B. J. Mariñas and A. M. Mayes, *Nature*, **452**, 301 (2008).
3. K. Kimura, G. Amy, J. E. Drewes, T. Heberer, T.-U. Kim and Y. Watanabe, *J. Membr. Sci.*, **227**, 113 (2003).
4. J. R. Werber, C. O. Osuji and M. Elimelech, *Nat. Rev. Mater.*, **1**, 16018 (2016).
5. M. Kumar, M. Grzelakowski, J. Zilles, M. Clark and W. Meier, *Proc. Natl. Acad. Sci. U.S.A.*, **104**, 20719 (2007).
6. M. Wang, Z. Wang, X. Wang, S. Wang, W. Ding and C. Gao, *Environ. Sci. Technol.*, **49**, 3761 (2015).
7. Y. Zhao, C. Qiu, X. Li, A. Vararattanavech, W. Shen, J. Torres, C. Hélix-Nielsen, R. Wang, X. Hu and A. G. Fane, *J. Membr. Sci.*, **423-424**, 422 (2012).
8. Y. X. Shen, P. O. Saboe, I. T. Sines, M. Erbakan and M. Kumar, *J. Membr. Sci.*, **454**, 359 (2014).
9. C. Y. Tang, Y. Zhao, R. Wang, C. Hélix-Nielsen and A. G. Fane, *Desalination*, **308**, 34 (2013).
10. X. Li, R. Wang, F. Wicaksana, C. Tang, J. Torres and A. G. Fane, *J. Membr. Sci.*, **450**, 181 (2014).
11. C. J. Huang, L. C. Wang, C. Y. Liu, A. S. T. Chiang and Y. C. Chang, *Biointerphases*, **9**, 029010 (2014).

12. J. L. Wu, Q. P. Wu, Y. P. Peng and J. M. Zhang, *Physiol. Res.*, **329**, 60 (2011).
13. K. Aquilano, S. Baldelli and M. R. Ciriolo, *Front. Pharmacol.*, **196**, 5 (2014).
14. E. Beitz, B. Wu, L. M. Holm, J. E. Schultz and T. Zeuthen, *Proc. Natl. Acad. Sci. U.S.A.*, **103**, 269 (2006).
15. T. Gonen and T. Walz, *Q. Rev. Biophys.*, **39**, 361 (2006).
16. L. Yu, Y. Zhang, Y. Wang, H. Zhang and J. Liu, *J. Hazard. Mater.*, **287**, 373 (2015).
17. J. Zhu, M. Tian, J. Hou, J. Wang, J. Lin, Y. Zhang, J. Liu and B. V. D. Bruggen, *J. Mater. Chem. A.*, **4**, 1980 (2015).
18. T. He, M. Frank, M. H. V. Mulder and M. Wessling, *J. Membr. Sci.*, **307**, 62 (2008).
19. S. M. Xue, Z. L. Xu, Y. J. Tang and C. H. Ji, *ACS Appl. Mater. Interfaces*, **8**, 19135 (2016).
20. J. Zhu, L. Qin, A. A. Uliana, J. Hou, W. Jing, Y. Zhang, L. Xin, S. Yuan, L. Jian and M. Tian, *ACS Appl. Mater. Interfaces*, **9**, 1975 (2017).
21. E. H. Wong, J. Kim, J. P. Scofield, P. Gurr, S. Kentish and G. Qiao, *J. Mater. Chem. A.*, **2**, 17751 (2014).
22. X. Yao, L. Guo, X. Chen, J. Huang, M. Steinhart and Y. Wang, *ACS Appl. Mater. Interfaces*, **7**, 6974 (2015).
23. D. H. N. Perera, Q. Song, H. Qiblawey and E. Sivaniah, *J. Membr. Sci.*, **487**, 74 (2015).
24. A. K. Ghosh, B. H. Jeong, X. Huang and E. M. V. Hoek, *J. Membr. Sci.*, **311**, 34 (2008).
25. W. Zhao, Y. Su, C. Li, Q. Shi, X. Ning, Z. Jiang, W. Zhao, Y. Su, C. Li, Q. Shi, X. Ning and Z. Jiang, *J. Membr. Sci.*, **318**, 405 (2008).
26. Y. Li, Y. Su, J. Li, X. Zhao, R. Zhang, X. Fan, J. Zhu, Y. Ma, Y. Liu and Z. Jiang, *J. Membr. Sci.*, **476**, 10 (2015).
27. A. Tiraferri, C. D. Vecitis and M. Elimelech, *ACS Appl. Mater. Interfaces*, **3**, 2869 (2011).
28. S. Y. Kwak and D. W. Ihm, *J. Membr. Sci.*, **158**, 143 (1999).
29. L. Fan, Q. Zhang, Z. Yang, R. Zhang, Y. N. Liu, M. He, Z. Jiang and Y. Su, *ACS Appl. Mater. Interfaces*, **9**, 15 (2017).
30. C. Bellona, J. E. Drewes, P. Xu and G. Amy, *Water Res.*, **38**, 2795 (2004).
31. M. He, K. Gao, L. Zhou, Z. Jiao, M. Wu, J. Cao, X. You, Z. Cai, Y. Su and Z. Jiang, *Acta Biomater.*, **40**, 142 (2016).
32. J. Wu and S. Chen, *Langmuir*, **28**, 2137 (2012).
33. S. Jiang and Z. Cao, *Adv. Mater.*, **22**, 920 (2010).
34. J. J. Wang, H. C. Yang, M. B. Wu, X. Zhang and Z. K. Xu, *J. Mater. Chem. A.*, **5**, 31 (2017).
35. M. He, K. Gao, L. Zhou, Z. Jiao, M. Wu, J. Cao, X. You, Z. Cai, Y. Su and Z. Jiang, *Acta Biomater.*, **40**, 142 (2016).
36. J. Wu and S. Chen, *Langmuir*, **28**, 2137 (2012).
37. X. M. Wang, B. Li, T. Zhang and X. Y. Li, *Desalination*, **370**, 7 (2015).
38. M. Liu, S. Yu, J. Tao and C. Gao, *J. Membr. Sci.*, **325**, 947 (2008).
39. D. Hu, Z. L. Xu and C. Chen, *Desalination*, **301**, 75 (2012).
40. O. Labban, C. Liu, T. H. Chong and H. L. V. John, *J. Membr. Sci.*, **521**, 18 (2017).
41. Y. J. Tang, Z. L. Xu, S. M. Xue, Y. M. Wei and H. Yang, *J. Membr. Sci.*, **538**, 9 (2017).
42. Q. F. An, W. D. Sun, Q. Zhao, Y. L. Ji and C. J. Gao, *J. Membr. Sci.*, **431**, 171 (2013).
43. H. Zhang, B. Li, J. Pan, Y. Qi, J. Shen, C. Gao and B. V. D. Bruggen, *J. Membr. Sci.*, **539**, 128 (2017).
44. D. Zhao, S. Yu, G. Liu, Q. Yuan and H. Guo, *Sep. Purif. Technol.*, **153**, 43 (2015).
45. M. Liu, C. Zhou, B. Dong, Z. Wu, L. Wang, S. Yu and C. Gao, *J. Membr. Sci.*, **463**, 173 (2014).
46. H. Li, W. Shi, Y. Zhang, Q. Du, X. Qin and Y. Su, *Sep. Purif. Technol.*, **166**, 240 (2016).
47. Q. Xie, W. Shao, S. Zhang, Z. Hong, Q. Wang and B. Zeng, *RSC Adv.*, **7**, 54898 (2017).
48. G. S. Lai, W. J. Lau, S. R. Gray, T. Matsuura, R. J. Gohari, M. N. Subramanian, S. O. Lai, C. S. Ong, A. F. Ismail and D. Emazadah, *J. Mater. Chem. A.*, **4**, 4134 (2016).
49. L. Li, S. Zhang and X. Zhang, *J. Membr. Sci.*, **335**, 13 (2009).
50. H. Wu, B. Tang and P. Wu, *J. Membr. Sci.*, **428**, 341 (2013).

Supporting Information

Improved performance of polyamide nanofiltration membranes by incorporating reduced glutathione during interfacial polymerization

Zhiwei Jiao*,, Linjie Zhou*,**, Mengyuan Wu*,**, Kang Gao*,**, Yanlei Su*,**,†, and Zhongyi Jiang*,****

*Key Laboratory for Green Chemical Technology, School of Chemical Engineering and Technology, Tianjin University, Tianjin 300072, China
**Collaborative Innovation Center of Chemical Science and Engineering (Tianjin), Tianjin University, Tianjin 300072, China
(*Received 23 October 2017 • accepted 18 September 2018*)

Table S1. Molecular weights, CAS numbers and purities of used dyes

Generic name	Molecular weight (g mol^{-1})	CAS number	Purity (%)
Orange GII	452.37	1936-15-8	95
Congo Red	696.67	573-58-0	75
Methyl blue	799.80	28983-56-4	90

Table S2. Chemical names and structures of dyes used in the experiment

Generic name	Chemical name	Chemical structure
Orange GII	1-Phenylazo-2-naphthol-6,8-disulfonic acid disodium salt	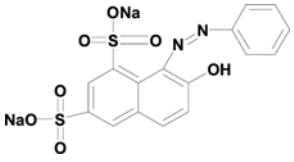
Congo red	Disodium 4-amino-3-[4-[4-[(1-amino-4-sulfonato-2-naphthyl)azo]phenyl]phenyl]azonaphthalene-1-sulfonate	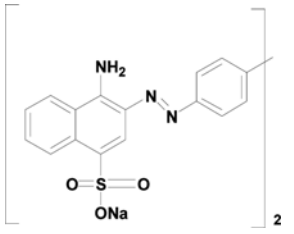
Methyl blue	Sodium triphenyl-p-rosanilne trisulfonate	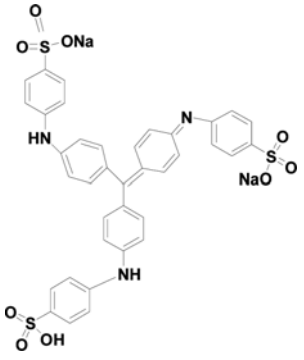

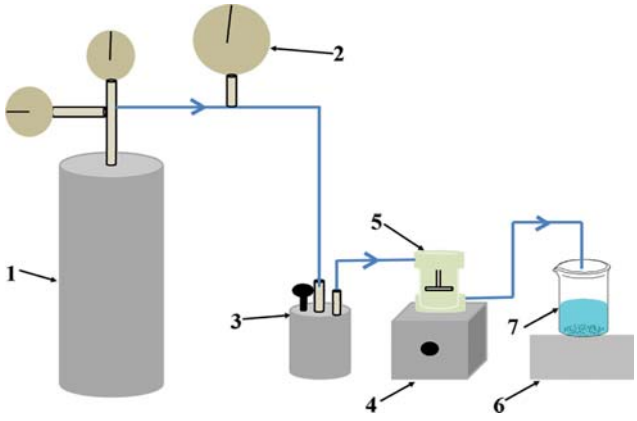

Fig. S1. Schematic illustration of the filtration cell setup.
1. Nitrogen cylinder
2. Precise pressure gauge
3. Pressure buffer
4. Magnetic stirrer
5. Filtration cell
6. Electronic scale
7. Beaker

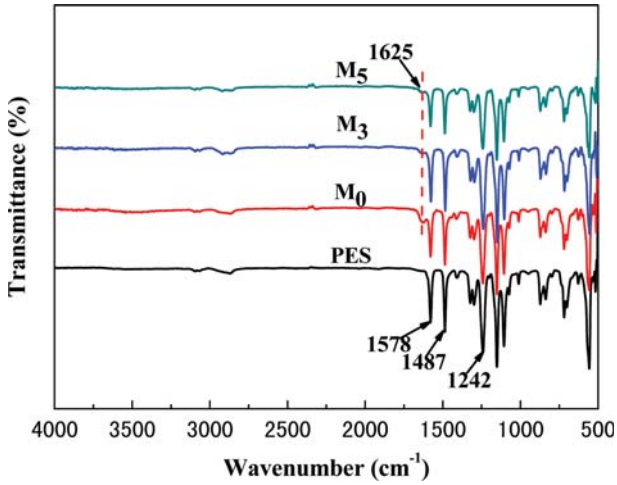

Fig. S2. FTIR spectra of PES, PIP-TMC NF membrane (M_0) and GHS/PIP-TMC NF membranes (M_3 with the addition of GHS was 20%, M_5 with the addition of GHS was 30%).

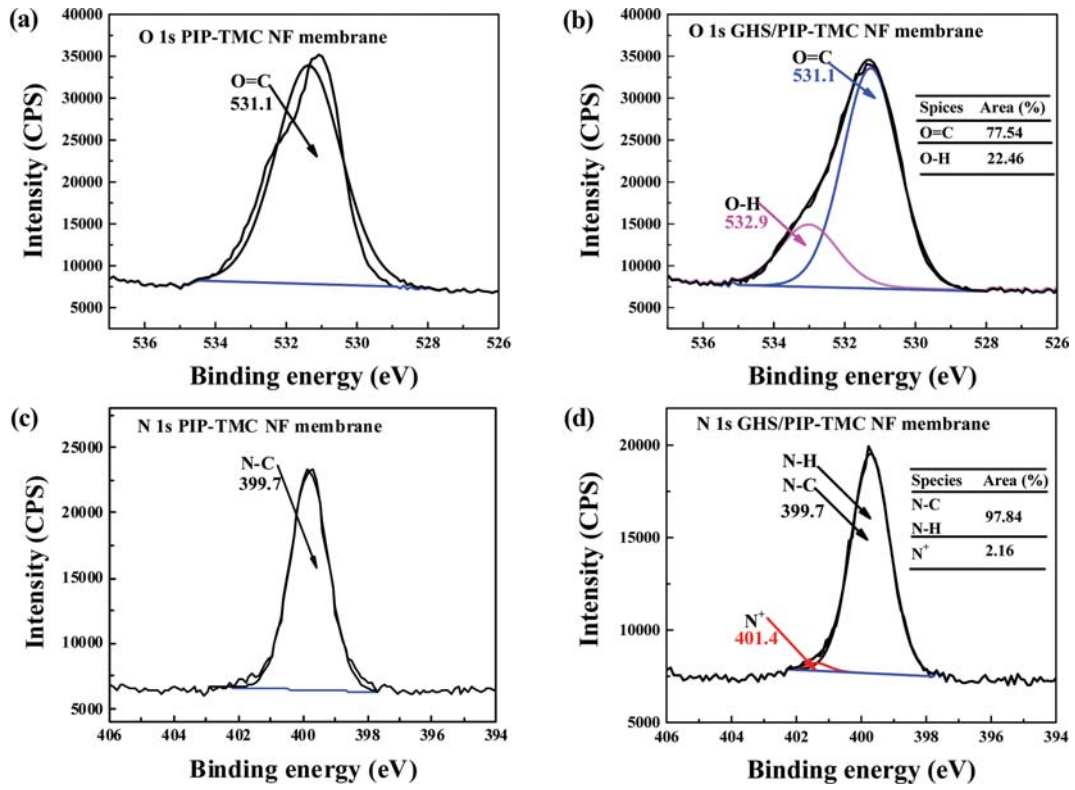

Fig. S3. High-resolution O 1s core level spectra of (a) PIP-TMC NF membrane (M_0), (b) GHS/PIP-TMC NF membrane (M_5), and high-resolution N 1s core level spectra of (c) PIP-TMC NF membrane (M_0), (d) GHS/PIP-TMC NF membrane (M_5).

ATR-FTIR was applied to measure the changes in chemical structures of the active layers of the NF membranes, Fig. S2 shows the ATR-FTIR spectra of FES, PIP-TMC (M_0), GHS/PIP-TMC NF membranes (M_3, M_5), all the membranes exhibited almost identical stretching vibration at 1,578 cm^{-1}, 1,487 cm^{-1} and 1,242 cm^{-1}, which were attributed to the stretching vibration of benzene ring, C-C bond and aromatic ether bond, respectively [1,2]. A characteristic peak appeared at 1,625 cm^{-1} of M_0, M_3 and M_5 membranes, corresponding to the stretching vibration peak of C=O bond in the amide group [3]. However, the -S-C=O deformation vibration was not obvious enough so that no sufficient evidence verified the existing of -S-C=O bond in the polyamide active layers of GHS/PIP-TMC NF membranes from ATR-FTIR spectra. Therefor this result could not confirm that successful incorporation of GHS into the polyamide active layer.

The O 1s core-level spectrum of PIP-TMC NF membrane (M_0) and GHS/PIP-TMC NF membrane (M_5) are shown in Fig. S3(a) and Fig. S3(b), only one peak appeared at 531.1 eV in the deconvolution of O 1s in PIP-TMC NF membrane (M_0), representing O=C bond. While in the deconvolution of O 1s in GHS/PIP-TMC NF membrane (M_5), the binding energy at 531.1 and 532.9 eV could be assigned to the O in the O=C and O-H bonds. As shown in Fig. S3(c), the N 1s score-level spectrum of PIP-TMC NF membrane (M_0) contained one main peak at 399.7 eV, according to the electron-withdrawing ability of the elements, the peak of 399.7 eV corresponded to N-C bond. As exhibited in the Fig. S3(d), the N 1s spectrum of GHS/PIP-TMC NF membrane (M_5) was deconvoluted into two peaks with the binding energy of 399.7 and 401.4 eV, which were attributed to the nitrogen atoms in the N-C, N-H bonds and protonated nitrogen atoms.

REFERENCES

1. A. Rahimpour, *Desalination*, **265**, 93 (2011).
2. K. R. Reddy, K. P. Lee and A. I. Gopalan, *J. Appl. Polym. Sci.*, **106**, 1181 (2007).
3. Y. Li, Y. Su, J. Li, X. Zhao, R. Zhang, X. Fan, J. Zhu, Y. Ma, Y. Liu and Z. Jiang, *J. Membr. Sci.*, **476**, 10 (2015).